Errors in Infiltration Calculations in Volume-Balance Models

E. Bautista, A.M.ASCE[1]; T. S. Strelkoff, M.ASCE[2]; and A. J. Clemmens, M.ASCE[3]

Abstract: Volume-balance models of surface irrigation calculate the infiltrated volume at a given time as a product of the stream length, upstream infiltration, and shape factors. The best-known expression of this type was derived by combining the Lewis-Milne equation with empirical power-law expressions for infiltration and advance as functions of time. This expression results in systematic errors that are not well understood by users of volume-balance methods. This article examines those errors in furrow irrigation by comparison with infiltrated volumes computed with zero-inertia simulation. The potential for errors is greatest with light soils and where the bottom slope is large enough to produce kinematic flow conditions. An example is presented to show how these errors in a parameter-estimation problem based on a volume balance can be corrected iteratively with the help of zero-inertia simulation. **DOI: 10.1061/(ASCE)IR.1943-4774.0000462.**
© 2012 American Society of Civil Engineers.

CE Database subject headings: Surface irrigation; Infiltration; Simulation models; Hydraulic models; Analytical techniques; Errors.

Author keywords: Surface irrigation; Infiltration; Simulation models; Hydraulic models; Analytical techniques.

J. Irrig. Drain Eng. 2012.138:727-735.
Downloaded from ascelibrary.org by Eduardo Bautista on 08/01/12. For personal use only.
No other uses without permission. Copyright (c) 2012. American Society of Civil Engineers. All rights reserved.

Introduction

In volume-balance calculations of surface irrigation, the infiltrated volume $V_z[L^3]$ at a given time is commonly calculated with an expression derived from the Lewis and Milne (1938) equation

$$V_Z(t) = \int_0^t Z(t - t_x)\frac{dx_A}{dt_x}dt_x \tag{1}$$

In the previous expression, Z = a function describing the infiltrated volume per unit length $[L^2]$ as a function of intake opportunity time, $\tau = t - t_x$; t = time elapsed since the beginning of the irrigation $[T]$; t_x = the time for the advancing wave of water to reach distance x_A $[L]$; and dx_A/dt_x = the derivative of a function describing advance distance as a function of time. The solution to Eq. (1) depends on the assumed functional forms for Z and $x_A(t_x)$ (Philip and Farrell 1964; Smerdon et al. 1988).

Assuming infiltration follows the empirical extended Kostiakov infiltration equation

$$Z = Wz = W(k\tau^a + b\tau) \tag{2}$$

and advance distance as a function of time follows a power law

$$x_A = pt^r \tag{3}$$

integration of Eq. (1) yields

$$V_z(t) = (RZ_1 \cdot kt^a + RZ_2 \cdot bt) \cdot W \cdot x_A(t) \tag{4}$$

In Eqs. (2) and (3), k$[L^2/T^a]$, a [−], b[L^{2}T], $p[L/T^r]$, and r [−] = empirical parameters, specific to the particular field conditions; and W [L] = transverse width (border/basin width, furrow spacing, or average wetted perimiter). Here, Eq. (4) relates V_z to the infiltrated volume per unit length at the upstream end of the field (where opportunity time = t) through the shape factors RZ_1 [−] and RZ_2 [−]. Expressions for RZ_1 and RZ_2 applicable during the advance phase are (Christiansen et al. 1966; Scaloppi et al. 1995)

$$RZ_1 = \frac{1 + a + r(1 - a)}{1 + a + r(1 + a)} \tag{5}$$

and

$$RZ_2 = \frac{1}{1 + r} \tag{6}$$

Eq. (5) is an approximation to the actual solution to the integral associated with the τ^a term, which is in the form of a gamma function (Strelkoff et al. 2009). During the postadvance phase, the subsurface shape factors RZ_1 and RZ_2 are given respectively by

$$RZ_1 = 1 + \sum_{i=1}^{N}\frac{-(t/t_L)^i r}{r + i}\prod_{j=0}^{i-1}\frac{a - j}{i - j} \tag{7}$$

and

$$RZ_2 = \left[1 - \frac{r(t/t_L)}{r + 1}\right] \tag{8}$$

Eqs. (7) and (8) were developed by Scaloppi et al. (1995) [corrected in Strelkoff et al. (2009)]. In Eq. (7), N = the number of terms used in the expansion; i and j = indices; and the operator $\prod$ denotes the product of i terms. The Eqs. (5) and (7) are functions of the constants a and r [the exponents of Eqs. (2) and (3), respectively] while Eqs. (6) and (8) are functions only of r.

[1]Research Hydraulic Engineer, USDA-ARS Arid Land Agricultural Research Center, 21881 N. Cardon Ln., Maricopa, AZ 85238 (corresponding author). E-mail: Eduardo.Bautista@ars.usda.gov

[2]Research Hydraulic Engineer, USDA-ARS Arid Land Agricultural Research Center, 21881 N. Cardon Ln, Maricopa, AZ 85238. E-mail: Theodor.Strelkoff@ars.usda.gov

[3]Senior Hydraulic Engineer, West Consultants, Inc., 8950 S. 52nd St., Suite 210, Tempe, AZ 85284-1043; formerly, Laboratory Director, USDA-ARS Arid Land Agricultural Research Center. E-mail: bclemmens@westconsultants.com

Note. This manuscript was submitted on March 8, 2011; approved on February 7, 2012; published online on February 9, 2012. Discussion period open until January 1, 2013; separate discussions must be submitted for individual papers. This paper is part of the ***Journal of Irrigation and Drainage Engineering***, Vol. 138, No. 8, August 1, 2012. ©ASCE, ISSN 0733-9437/2012/8-727–735/$25.00.

When combined with Eq. (4), the volume-balance model is given by

$$V_{in}(t) - V_y(t) - V_{ro}(t) = (RZ_1 \cdot kt^a + RZ_2 \cdot bt) \cdot W \cdot x_A(t) \quad (9)$$

Here V_{in}, V_y, and V_{ro} represent the inflow, surface storage, and runoff volumes, respectively, and $x_A = L_f$ (the field length) when $V_{ro} > 0$. This expression is frequently used to formulate parameter-estimation problems. In those applications, Eq. (9) is applied at two or more times with observed irrigation data (e.g., advance as a function of time, runoff) and used to solve for one or more unknown infiltration parameters. The value of r needed to solve for RZ_1 and RZ_2 is found by fitting the advance trajectory measured at discrete locations ($x_A - t_x$ data pairs) to Eq. (3). The estimated parameters are validated by feeding them into an unsteady-flow simulation model Users typically accept the estimated parameters when simulation outputs and field observations are in reasonable agreement. Differences between simulation results and observations generally are attributed to random or faulty field data. In either case, users often ignore potential biases in the computation of V_z. In particular, users of these computational procedures are aware that a power advance law often does not fit measured advance data adequately, but they are less clear about how this affects the accuracy of V_z estimates, and, in those cases, whether those estimates can be improved.

This article examines the relationship between infiltrated volumes predicted with the zero-inertia simulation model, and corresponding volumes computed with the power infiltration integral, Eq. (4). The objective is to quantify the potential magnitude of the volume-balance errors under a representative range of conditions, and to identify conditions under which those errors can be substantial. The analysis is confined to the advance phase of the irrigation, and to furrow irrigation with infiltration described by Eq. (2). The first part of the analysis examines the behavior of a shape factor σ_z characterizing the infiltration profile simulated with the zero-inertia model, as a function of advance distance under various hydraulic conditions. Here, σ_z is defined as the ratio

$$\sigma_z(x_A) = \frac{Z_{\text{avg}}}{Z_0(t)} \quad (10)$$

in which $Z_{\text{avg}} = V_z(t)/x_A(t)$ is the simulated average infiltration over the advance distance $x_A(t)$, and $Z_0(t)$ = the corresponding infiltration at the upstream end. The second part of the analysis examines the relationship between σ_z and the volume-balance shape factors, RZ_1 [Eq. (5)] and RZ_2 [Eq. (6)]. While RZ_1 and RZ_2 are constants, their relative contribution to $V_z(t)$ varies with time because they multiply different terms in Eq. (4). Hence, one can compare σ_z with σ_{z_PI}, the shape of the infiltrated profile computed with the power infiltration integral, Eqs. (4)–(6)

$$\sigma_{z\_PI} = \frac{(RZ_1 \cdot kt^a + RZ_2 \cdot bt)W}{Z_0(t)} \quad (11)$$

Finally, a strategy is presented for correcting errors associated with Eqs. (4)–(6) in parameter-estimation problems.

Methodology

The analysis uses dimensionless furrow-irrigation scenarios that were developed to represent a reasonable range of irrigation conditions. The dimensionless system of variables is described in a companion paper (Bautista et al. 2012). Dimensionless variables reduce the number of governing parameters and allow results to be generalized more easily. A dimensionless variable is obtained by dividing a dimensioned variable by a reference variable. For example, the dimensionless advance distance x_A^* is defined as $x_A^* = x_A/X_R$, where x_A is the dimensional distance and X_R the reference distance.

If Z is given by Eq. (2), then dimensionless advance ($x_A^* = x_A/X_R$) as a function of dimensionless time $t^*(t^* = t/T_R)$ can be expressed as a function of four dimensionless parameters $x_A^*(t^*) = f(K^*, a, B^*, D_0^*)$, defined as

$$K^* = \frac{WkT_R^a}{Y_R^2}; \qquad B^* = \frac{WbT_R}{Y_R^2}; \qquad D_0^* = \frac{A(Y_R)}{Y_R^2}\left[\frac{R(Y_R)}{Y_R}\right]^{2/3}\frac{n_R}{n} \quad (12)$$

In Eq. (12), T_R, Y_R, n_R = reference variables (time, vertical length, Manning roughness coefficient n); $A(Y_R)$ and $R(Y_R)$ = flow area and hydraulic radius as a function of Y_R, respectively;and all other dimensionesd variables are as previously defined; K^* and B^* = functions of the infiltration parameters k and b, respectively, but they are also functions of slope and discharge; D_0^* = a parameter related to the channel conveyance and a function of the cross-sectional geometry (the side slope SS and bottom width BW for a trapezoidal cross section).

To facilitate the interpretation of results and narrow the range of the dimensionless variables to explore, a basic set of 16 dimensionless scenarios was defined from a set of dimensional scenarios. The dimensional scenarios were defined from combinations of four slopes and four infiltration conditions, as given in Table 1. The table provides an identifier for each scenario, which are used later in this article to label graphical results. Infiltration was defined from the time t_{req} needed to infiltrate a prescribed application depth z_{req}. Furthermore, the following relationship was used to define b

$$b = \lambda \frac{z_{\text{req}}}{t_{\text{req}}} \quad (13)$$

In this expression, λ = a parameter that determines the relative contribution of b to the infiltrated depth at t_{req}. When $\lambda = 0$, Eq. (13) reduces to the Kostiakov equation, while $\lambda = 1$ implies a constant infiltration rate throughout the irrigation event.

The companion article (Bautista et al. 2012) explains the development of the dimensionless scenarios. An initial set of scenarios was developed with $a = 0.5$ and $\lambda = 0.4$. Thus, this set of scenarios assumes that 40% of the z_{req} at t_{req} is contributed by the steady-infiltration term. Two additional sets were generated with $a = 0.5$, but with $\lambda = 0.1$ and $\lambda = 1.0$. This third set was included to study the limiting case of water infiltrating at a constant rate. Two more sets of scenarios were developed with $\lambda = 0.4$, but with $a = 0.3$ and 0.7. The K^* and B^* values for all sets of scenarios ($\lambda = 0.4$, $a = 0.5$), ($\lambda = 0.1$, $a = 0.5$), ($\lambda = 1.0$, $a = 0.5$), and ($\lambda = 0.4$, $a = 0.3$) are given in Bautista et al. (2012). It is worth noting that changes to λ produce the same change in K^* (for all scenarios with the same slope) but have no effect on the dimensionless furrow lengths and D_0^* or its dimensional counterparts. In contrast, a change in the infiltration exponent produces variations in K^*

Table 1. Identifiers for the 16 Furrow-Irrigation Scenarios

	S_0			
t_{req} (h)	0.00001	0.0001	0.001	0.01
2	1	5	9	13
4	2	6	10	14
8	3	7	11	15
16	4	8	12	16

J. Irrig. Drain Eng. 2012.138:727-735.
Downloaded from ascelibrary.org by Eduardo Bautista on 08/01/12. For personal use only.
No other uses without permission. Copyright (C) 2012. American Society of Civil Engineers. All rights reserved.

of different magnitude with all scenarios. Thus, very different combinations of infiltration parameters can produce irrigation scenarios that are closely related.

Simulations were conducted with the zero-inertia engine of the WinSRFR surface irrigation analysis program (Bautista et al. 2009c). The program calculates σ_z at each time step with Eq. (10); these values were extracted from the output file.

That Z is given by Eq. (2) is relevant to the objectives of this study and merits further discussion. Unsteady flow simulation of furrow irrigation will produce different infiltration profiles when using an infiltration formulation that accounts for the variation in wetted perimeter with depth as opposed to a formulation that neglects those effects (Bautista and Wallender 1993). Hence, this assumption directly impacts the subsurface shape factors. However, because the goal is to improve the accuracy of volume-balance calculations, and those calculations currently cannot account for time-dependent wetted-perimeter infiltration effects, the results presented herein have practical value. Furthermore, efforts to measure time-dependent wetted-perimeter effects on infiltration in the field have produced inconclusive results, because of spatial and temporal variability of furrow cross section and hydraulic resistance, including erosion and deposition effects (Trout 1992; Walker and Kasilingam 2004).

Results

The σ_z Relationships as a Function of x_A

Here Fig. 1 illustrates the $\sigma_z(x_A^*)$ relationships for the scenarios developed with $\lambda = 0.4$, $a = 0.5$. The σ_z curves generated for the same K^* plot are close to each other when plotted as a function of $\log x_A^*$ because the order of magnitude of L_f^* is a function of S_0.

All curves exhibit the same fundamental behavior. During the initial advance, Z_0 grows more rapidly than Z_{avg} (and, therefore, σ_z decreases as a function of x_A^*) because the stream elongates rapidly while the infiltration rate at the field inlet is large. With increasing advance, distance and time, the infiltration rate at the inlet decreases while Z_{avg} grows slightly faster because of a decreasing stream advance rate. Hence, σ_z eventually increases.

For a given K^* (e.g., Scenarios 1–4), the effect of a decreasing B^* is to push the σ_z relationship upward and also to push the point where the slope of the relationship changes from negative to positive farther upstream, especially at small slopes. Smaller values of B^* (i.e., smaller infiltration rates for the same z_{req}) should be expected to produce more uniform infiltration profiles, and thus, larger values for σ_z. The effect of an increasing slope for scenarios with the same t_{req} (e.g., Scenarios 1, 5, 9, 13) is to increase the stream advance rate. A larger stream speed induces larger differences between Z_{avg} and Z_0 at small advance distances (and thus smaller σ_z values). For larger advance distances, a large stream speed reduces the differences in intake opportunity time (and thus, infiltrated volume per unit length) along the field. Hence, the range for σ_z increases with increasing slope.

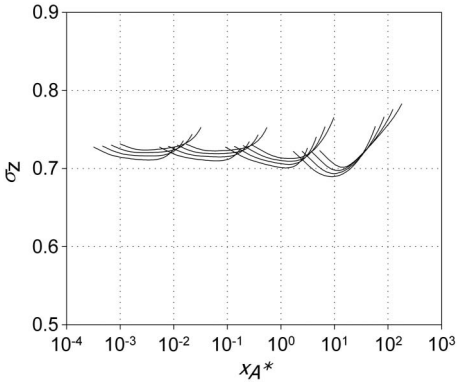

Fig. 1. Simulated subsurface shape factors as a function of dimensionless advance distance for the furrow-irrigation scenarios with $\lambda = 0.4$, $a = 0.5$

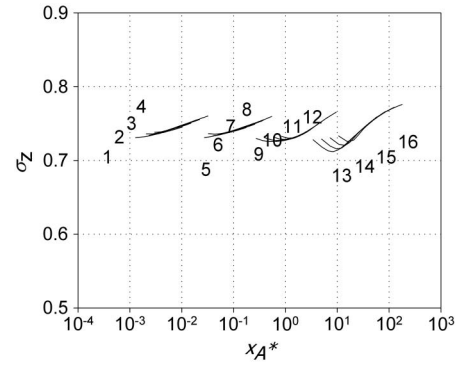

Fig. 2. Simulated subsurface shape factors as a function of dimensionless advance distance for the furrow-irrigation scenarios with $\lambda = 0.1$, $a = 0.5$

In Fig. 2, the $\sigma_z(x_A^*)$ relationship is depicted for the scenarios developed with $a = 0.5$, $\lambda = 0.1$. Curves generated for the same K^* plot closer to each other than in Fig. 1 and are difficult to tell apart. In contrast with the results generated with $\lambda = 0.4$ (Fig. 1), σ_z decreases over a shorter advance distance and the range of variation for σ_z is narrower. These scenarios involve short fields relative to the maximum advance distance ($0.1/B^*$). Beacuse σ_z attains its maximum value ($\sigma_z < 1$) at the maximum advance distance, field length limits the growth and, thus, the range of σ_z. Like the surface shape factor (Bautista et al. 2012), σ_z tends to have a constant value when $b = 0$ because $1/B^* = \infty$.

The behavior of the σ_z relationships when the infiltration rate is constant ($a = 0.5$, $\lambda = 1.0$) is illustrated in Fig. 3. Because the initial advance rate of the stream is much greater in these cases than for the scenarios of Figs. 1 and 2, σ_z decreases more sharply. When water infiltrates at a constant rate and the advance rate is large, the shape of the infiltrated profile approximates a triangle (i.e., $\sigma_z \to 0.5$). The slope of the σ_z relationship eventually changes as a result of a declining advance rate. Thereafter σ_z increases very rapidly because advance distance approximates $1/B^*$. In contrast to

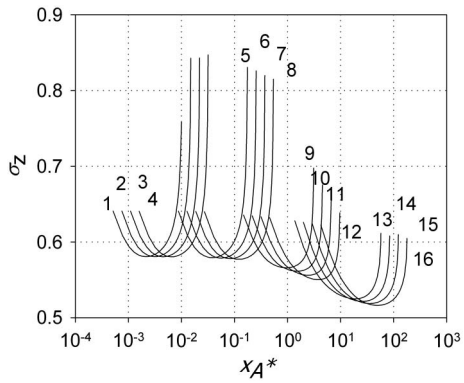

Fig. 3. Simulated subsurface shape factors as a function of dimensionless advance distance for the furrow-irrigation scenarios with $\lambda = 1.0$, $a = 0.5$

J. Irrig. Drain Eng. 2012.138:727-735.
Downloaded from ascelibrary.org by Eduardo Bautista on 08/01/12. For personal use only.
No other uses without permission. Copyright (c) 2012. American Society of Civil Engineers. All rights reserved.

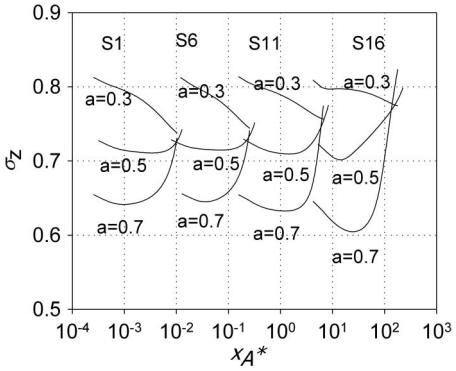

Fig. 4. Simulated subsurface shape factors as a function of dimensionless advance distance and the exponent a ($a = 0.3$, 0.5, and 0.7) for 12 furrow-irrigation scenarios ($\lambda = 0.4$)

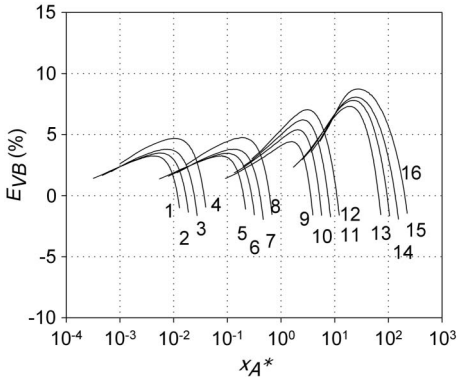

Fig. 5. Volume-balance errors computed with power-law shape factors for the furrow-irrigation scenarios with $\lambda = 0.4$, $a = 0.5$

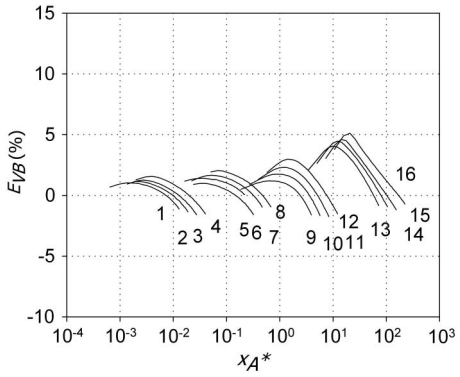

Fig. 6. Volume-balance errors computed with power-law shape factors for the furrow-irrigation scenarios with $\lambda = 0.1$, $a = 0.5$

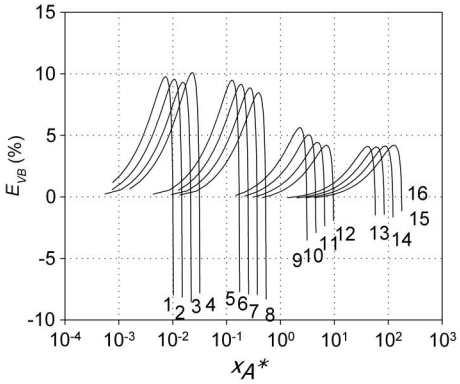

Fig. 7. Volume-balance errors computed with power-law shape factors for the furrow-irrigation scenarios with $\lambda = 1.0$, $a = 0.5$

the results of Figs. 1 and 2, the range of variation for σ_z increases as slope decreases. This is because of the very rapid decline in advance rate when the slope is small.

In Fig. 4, the σ_z relationships are compared for three values of the infiltration exponent a (0.3, 0.5, and 0.7) with $\lambda = 0.4$. Four of the scenarios from Table 1 are included in the graph (1, 6, 11, and 16). The relationships developed with $a = 0.7$ exhibit similar trends to those developed with $a = 0.5$; that is, σ_z first decreases but later increases as a function of x_A^*. The range of variation for σ_z is substantially greater when $a = 0.7$ than with $a = 0.5$, especially when the slope is large (S16). The relationships developed with $a = 0.3$ exhibit a very different behavior. In those cases, σ_z decreases as a function of distance (for the range of advance distances included in the analysis) and the range of variation decreases with increasing slope. When a is small, the infiltration rate at small times is large, and consequently, the initial advance is slow. However, the advance rate tends to remain constant because transient infiltration effects dissipate quickly. If the stream elongates at a relatively constant rate, then Z_{avg} cannot grow very fast relative to Z_0. Thus, σ_z decreases over a longer advance distance when a is small. When a is large, advance is initially fast but slows down rapidly because transient infiltration effects persist. The pronounced stream deceleration explains the subsequent rapid increase in σ_z.

Relationship between the Simulated and Volume-Balance Shape Factors

The first question examined in this section is the magnitude of the errors resulting from the application of Eq. (4) as a function of x_A^*. Those errors are quantified in relation to the infiltrated volumes computed with zero inertia as follows.

Volume-balance errors E_{VB} were calculated for each set of scenarios presented in Figs. 1–4; E_{VB} is defined as

$$E_{VB} = \frac{V_{z\_PI} - V_{z\_ZI}}{V_{in}} \times 100 \tag{14}$$

In Eq. (14), V_{z_PI} = the infiltrated volume computed with the power-law integral; V_{z_ZI} = the corresponding volume computed with zero-inertia simulation; and V_{in} = the inflow volume. In this expression the V_{z_PI}, V_{z_ZI}, and V_{in} are evaluated at $t^*(x_A^*)$. The advance exponent r needed by the power-law integral was calculated from the simulated advance trajectories. The simulated $x_A - t_x$ data pairs were fitted to Eq. (3) using nonlinear regression. Results are presented in Figs. 5–8. Regression r^2 values exceeded 0.99 except for the scenarios illustrated in Fig. 7 and in Fig. 8, $a = 0.7$.

These results show, first, that the power-law integral generally overestimates V_z except when $x_A^* B^*$ is close to L_f^*. The error at $x_A^* = L_f^*$ generally is small but negative. Under the range of conditions examined herein, the absolute value of E_{VB} generally is less than 5% but errors can exceed 10%. Systematic differences between the volume-balance and zero-inertia infiltration volumes translate into differences between the observed advance and advance predicted with the zero-inertia model, independent of erroneous inputs and/or random field properties. Hence, these errors affect the ability

J. Irrig. Drain Eng. 2012.138:727-735.
Downloaded from ascelibrary.org by Eduardo Bautista on 08/01/12. For personal use only.
No other uses without permission. Copyright (C) 2012. American Society of Civil Engineers. All rights reserved.

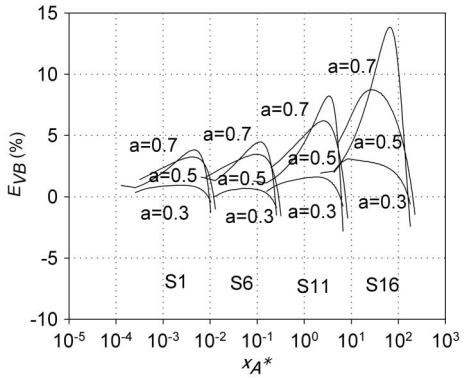

Fig. 8. Volume-balance errors computed with power-law shape factors for the furrow-irrigation scenarios with $\lambda = 0.4$, $a = 0.3$, 0.5, and 0.7

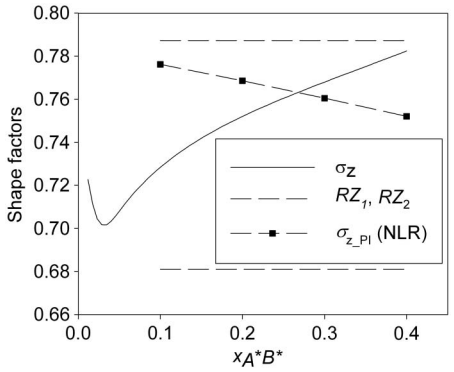

Fig. 9. Relationship between σ_z, (RZ_1, RZ_2), and σ_{z_PI} for Scenario 16, $\lambda = 0.4$, $a = 0.5$

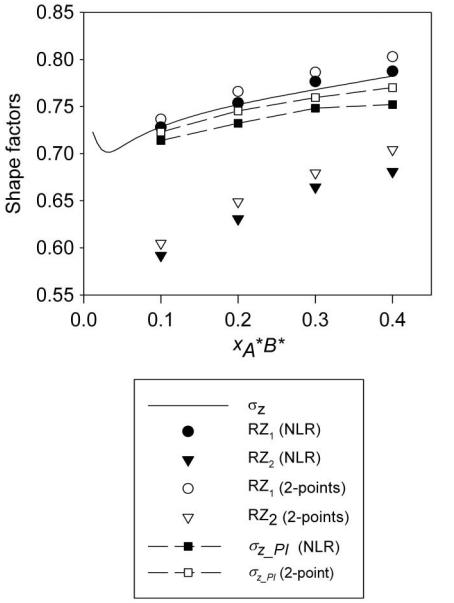

x_{Arel}^*	0.1	0.2	0.3	0.4
r (NLR)	0.689	0.586	0.505	0.469
r (2-point	0.653	0.541	0.472	0.420

Fig. 10. Effect of the data and method used to calculate the advance exponent r on the relationship between σ_z, (RZ_1, RZ_2), and σ_{z_PI} for Scenario 16, $\lambda = 0.4$, $a = 0.5$

to validate infiltration parameter estimates with zero-inertia simulation.

Because E_{VB} varies with x_A^*, the relative magnitude of the errors should be considered in selecting locations at which to compute volume-balance relationships. In the examples of Figs. 5 and 6, E_{VB} peaks at short advance distances but decreases thereafter (this is not entirely evident from the graphs, because of the logarithmic scale for x_A^*). These results suggest that short advance distances should be avoided when calculating volume-balance relationships. However, the results of Figs. 7 and 8 show that Eq. (4) can be very inaccurate when applied near the maximum advance distance if λ and/or a are large. For example, if the well-known Elliott and Walker (1982) two-point parameter-estimation method is applied to the conditions of Fig. 8 (Scenario 16, $\lambda = 0.4$, $a = 0.7$), then the middle of the field corresponds to the location with the largest E_{VB}. The error can be reduced by calculating a volume balance, say, at three-quarters of the field length, although the error is still substantial.

The results of Figs. 5–7, in combination with those of Figs. 1–3, suggest that the potential magnitude of errors increases as the range of σ_z increases. The results of Figs. 8 and 4 show this is not always the case. The σ_z varies over a wider range for scenarios generated with $a = 0.3$, $\lambda = 0.4$ (Fig. 4) than for scenarios generated with $a = 0.5$, $\lambda = 0.4$ (Fig. 4), but the corresponding volume-balance errors are smaller (Fig. 8). Similarly, σ_z varies over a much wider range for scenarios generated with $a = 0.5$ and $\lambda = 1$ (Fig. 3) than for scenarios ($a = 0.7$, $\lambda = 0.4$) (Fig. 4), but the peak error is greater with the latter ($E_{VB} \approx 14\%$) (Fig. 8). The following paragraphs explore the nature of these errors.

In Fig. 9, the relationship between σ_z, the power-law shape factors, and σ_{z_PI} for Scenario 16 of Fig. 1 ($\lambda = 0.4$, $a = 0.5$) is examined. Results are plotted as a function of a new dimensionless variable, $x_A^*B^*$, the ratio of the dimensionless advance distance and the theoretical maximum distance that water can advance under the given conditions. Recall that the dimensionless field lengths for these scenarios were determined as $L_f^* = \lambda/B^*$, Therefore, in Fig. 9 (and in the figures that follow), the maximum value of $x_A^*B^*$ is the relative dimensionless field length $L_f^*/(1/B^*) = \lambda$. In addition, RZ_1 and RZ_2 were used to determine σ_{z_PI} at $x_A^*B^* = 0.1$, 0.2, 0.3, and 0.4. In the figure, the solid line represents σ_z, the dashed lines RZ_1 and RZ_2, and the filled squares with dashed lines represent σ_{z_PI}. While σ_z is mostly an increasing function of $x_A^*B^*$, σ_{z_PI} is a decreasing function. The slope of σ_{z_PI} is necessarily negative, first because RZ_1 is always larger than RZ_2, and second because the contribution of RZ_1 to V_z diminishes with time because it multiplies the transient term kt^a. Thus, the power integral cannot represent the evolution of σ_z when σ_z is an increasing function of $x_A^*B^*$.

Because flow deceleration is more extreme with increasing advance distance, estimates of r decrease as the advance distance used to fit Eq. (3) increases. Smaller values of r translate into larger values for the shape factors. This implies that the slope of σ_{z_PI} can be made positive by using a variable value of r, that is, by recalculating r with increasing advance distance (with r calculated with nonlinear regression). This is illustrated in Fig. 10. Power advance relationships were developed from field segments of increasing length, corresponding to $x_A^*B^*$ values of 0.1, 0.2, and 0.3. These r values were used to compute the shape factors, which are displayed in the figure along with the values previously computed for $x_A^*B^* = 0.4$ [RZ_1 (NLR) = filled circle, and RZ_2 (NLR) = filled triangle]. As expected, the shape factors and the resulting σ_{z_PI} (filled square with dashed line) increase with distance and track $\sigma_z(x_A^*B^*)$ better

Downloaded from ascelibrary.org by Eduardo Bautista on 08/01/12. For personal use only.
No other uses without permission. Copyright (c) 2012. American Society of Civil Engineers. All rights reserved.
J. Irrig. Drain Eng. 2012.138:727-735.

J. Irrig. Drain Eng. 2012.138:727-735.
Downloaded from ascelibrary.org by Eduardo Bautista on 08/01/12. For personal use only.
No other uses without permission. Copyright (c) 2012. American Society of Civil Engineers. All rights reserved.

than by using a constant value of r. In fact, for this example, RZ_1 (NLR) nearly matches σ_z.

In addition to the length of the advance trajectory, r depends on the number of measured data points and the method used to fit the data. In practice, the advance trajectory is often measured using only two data pairs, one located in the middle of the field and the other at the end of the field. These data can be combined with the log transform of Eq. (3) to set up a system of two linear equations and unknowns. Of interest, then, is the exploration of how results are affected by using this two-point technique.

Power advance relationships were developed using the two-point method for the same field segments as before ($x_A^* B^* = 0.1$, 0.2, 0.3, and 0.4). Because the two-point method ignores the early part of the advance trajectory, when velocities are larger, r values are smaller than those computed with regression. Hence, the resulting shape factors [RZ_1 (2-point) = empty circle, and RZ_2 (2-point) = empty triangle] are larger than the values derived from nonlinear regression (Fig. 10). As a result, the corresponding σ_{z_PI} (two-point) series (empty squares with dashed line) is closer to the σ_z relationship than the σ_{z_PI} (NLR) series.

Three additional scenarios were examined, Scenario 1 $\lambda = 1.0$, $a = 0.4$ (Fig. 11), Scenario 1, $\lambda = 0.4$, $a = 0.3$ (Fig. 12), and Scenario 16, $\lambda = 0.4$, $a = 0.7$ (Fig. 13). The figures depict σ_z, σ_{z_PI} calculated with a constant r (r calculated using advance to the end of the field, $x_A^* B^* = \lambda$) and the shape factors calculated with variable r (r updated with increasing advance distance),

When $\lambda = 1.0$, $\sigma_{z\_PI} \equiv RZ_2$. If the power infiltration integral is applied under those conditions with a constant r, it will necessarily and substantially overestimate infiltration except when close to $x_A^* B^* = \lambda$ (Fig. 11). Calculations at $x_A^* B^* = \lambda$ result in an absolute error in excess of 5%, because of the extreme nonlinearity of the advance trajectory. More accurate V_Z estimates can be developed at shorter advance distances if r is updated as a function of advance distance.

The σ_z and σ_{z_PI} relationships are in close agreement for Scenario 1, $\lambda = 0.4$, $a = 0.3$ (Fig. 12), a case for which the slope of the σ_z relationship is negative (for the field length considered in the analysis). For this example, the range of r values fitted from different advance segments is much narrower than for the examples of Figs. 10 and 11. Because r values are not very different, the shape factors are also very similar with increasing advance distance. Similarly, r values calculated with only two advance points are not very different from those calculated with multiple data points and regression, at least for the range of distances illustrated in Fig. 12.

In contrast with the previous example, the advance trajectory is initially fast but very nonlinear when $\lambda = 0.4$, $a = 0.7$ (Fig. 13).

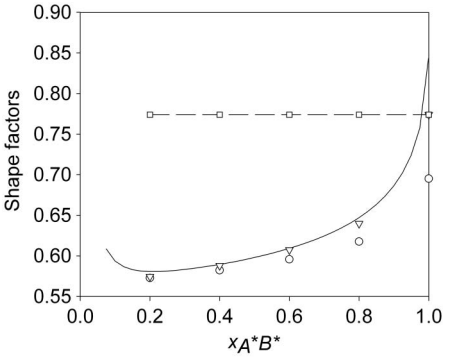

x_{Arel}^*	0.2	0.4	0.6	0.8	1.0
r (NLR)	0.746	0.718	0.679	0.620	0.439
r (2-point	0.741	0.701	0.647	0.563	0.292

Fig. 11. Relationship between σ_z, (RZ_1, RZ_2), and σ_{z_PI} for Scenario 1, $\lambda = 1.0$, $a = 0.5$

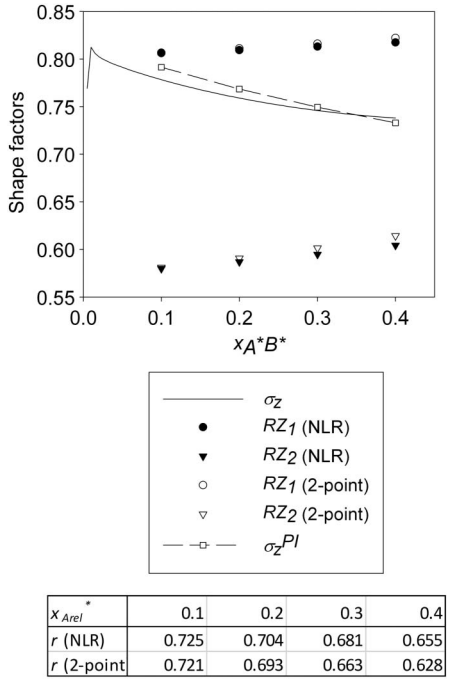

x_{Arel}^*	0.1	0.2	0.3	0.4
r (NLR)	0.725	0.704	0.681	0.655
r (2-point	0.721	0.693	0.663	0.628

Fig. 12. Relationship between σ_z, (RZ_1, RZ_2), and σ_{z_PI} for Scenario 1, $\lambda = 0.4$, $a = 0.3$

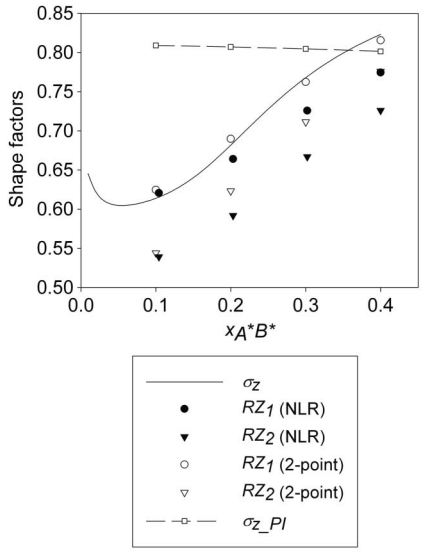

x_{Arel}^*	0.1	0.2	0.3	0.4
r (NLR)	0.855	0.690	0.500	0.377
r (2-point	0.838	0.605	0.406	0.289

Fig. 13. Relationship between σ_z, (RZ_1, RZ_2), and σ_{z_PI} for Scenario 1, $\lambda = 0.4$, $a = 0.7$

This is indicated by the range of r values given in the figure. The slope of the σ_z relationship is mostly positive and varies over a wide range, and thus the differences between σ_z and σ_{z_PI} are more extreme than for the example of Fig. 9. The difference between σ_z and σ_{z_PI} is greatest at $x_A^* B^* = 0.1$, but the corresponding E_{VB} is greatest at $x_A^* B^* = 0.2$. When $x_A^* B^* = 0.1$, the infiltrated volume relative to the applied volume is small and, thus, translates into a small value of E_{VB}. Unlike the results of Fig. 10, the shape factors calculated for this example with nonlinear regression do not bracket the σ_z relationship, even for short advance distances. Thus, use of nonlinear regression to calculate r seems more questionable than with previous examples.

Discussion

The above results assume perfect knowledge of advance distance as a function of time. In practice, field-measured advance data can be erratic and the computed r can be very sensitive to one or more data points. Hence, values of r calculated for increasing advance distances may fail to decrease monotonically. Similarly, values of r computed from two advance measurements may fail to adequately represent the observed advance trajectory. In those cases, use of multiple advance data and nonlinear regression may still be the recommended approach for estimating r (McClymont and Smith 1996)

Additional simulations, which are not documented here, suggest that the slope of σ_z relationship tends to remain negative for longer advance distances when $a < 0.5$ and becomes positive at short distances when $a > 0.5$. Of interest then is the range of a values that can be encountered in practical field situations. Recent simulation studies have generated one-dimensional infiltration solutions based on the governing equations of unsaturated porous media flow, for different initial and boundary conditions, and fitted those results to the extended Kostiakov equation (Furman et al. 2006; Valiantzas et al. 2009). Those results suggest that a is generally less than 0.5, but larger values were also computed with light soils. The new National Resources Conservation Service (NRCS) infiltration functions (Walker et al. 2006), which were developed mostly from field-measured furrow-irrigation data, have a values that range from 0.188 to 0.749, with low values associated with heavy soils and large values associated with light soils. Light soils are also conditions under which the steady state term in Eq. (2) can be expected to be relatively large. These results imply that the potential for inaccurate V_z estimates with Eq. (4) is greatest with light soils, and further increases if the slope is large.

Iterative Use of the Infiltration Power-Law Integral with Zero-Inertia Simulation

The above results show that Eq. (4) can be inaccurate relative to zero-inertia model infiltration predictions under some field conditions. Results of a volume-balance analysis need to be interpreted carefully, at the very least, under those conditions. The analysis shows that the accuracy of volume-balance results can be improved by updating the value of r with advance distance, but as noted in the previous section, those values when derived from field data may not vary monotonically. Another complication in the application of the volume-balance model is that surface-volume estimates required by Eq. (9) are also uncertain (Bautista et al. 2012). Those estimates generally are derived as follows:

$$V_y = \sigma_y A_0 x_A \tag{15}$$

In this expression, σ_y = a surface profile shape factor and A_0 = the upstream cross-sectional flow area. Typical applications of Eq. (15) assume normal depth for the calculation of A_0 and a constant σ_y. Given these constraints, a better alternative for refining V_z estimates is to iterate the volume-balance calculations using zero-inertia simulated σ_z values instead of the shape factors given by Eqs. (5)–(8). The same simulation data can be also used to refine the V_y estimates. The following example illustrates the procedure as applied to a parameter-estimation problem.

The example corresponds to the Printz 3-2-3 furrow, originally reported in Elliott (1980), and later analyzed in Bautista et al. (2009b). Inputs for this example are $L_f = 350$ m; $Q = 3.75$ l/s with a 110-min cutoff time; $S_0 = 0.0025$; $BW = 0.14$ m; $SS = 1.61$; $W(\text{furrow spacing}) = 1.52$ m; and $n = 0.025$. The given discharge and slope are average values. With the given data, the applied depth was 46.5 mm while the infiltrated depth calculated from the final volume balance was 44 mm.

A parameter-optimization procedure was set up in a spreadsheet, using the advance times to the middle and end of the field and cutoff time. The methodology, described in Bautista et al. (2009a), searches for a parameter combination that minimizes the squared difference between the left-hand side of Eq. (9) (the measured infiltration) and the right-hand side (the predicted infiltration). Although all three parameters of Eq. (2) are unknown, the example is based on optimization of k and b only, with $a = 0.5$. The procedure can be repeated with other values of a if further potential improvements in the solution need to be examined.

Table 2 shows the advance times and inflow and runoff volumes needed for application of Eq. (9). Iteration results are presented in Table 3. The upstream depth y_0 needed to determine surface storage was calculated using the procedures described in Bautista et al. (2012). In the first iteration, RZ_1/RZ_2 and a reasonable estimate of the surface shape factor σ_y were used to determine V_z and V_y, respectively. These values were used to determine a first set of infiltration parameters k and b. This solution was tested with simulation, using the measured hydrograph and field elevations as a function of distance. The goodness of fit of the estimated infiltration function was evaluated, in this example, by comparing the measured and simulated infiltrated depths (z) and runoff hydrographs. The Nash-Sutcliffe efficiency indicator (NSE) (Nash and Sutcliffe 1970) was used to compare runoff values. The first iteration yielded an infiltrated depth of 40 mm and a low value for NSE (-1.62). A second zero-inertia simulation was conducted with the estimated parameters, but with average discharge and slope. This step is needed because surface-volume computations assume a depth profile that varies gradually as a power law of distance (Bautista et al. 2012). Values for the subsurface and surface shape factors, σ_z and σ_y, computed at L_f and $L_f/2$ (Table 3) were extracted from the simulation results and provided as inputs to the second iteration of the parameter optimization procedure. The sequence of computations was carried out three additional times. The second iteration produced substantial improvements in both the predicted infiltrated depth and the NSE indicator (Table 3). The third iteration produced a slight improvement in the predicted infiltrated depth, but a decrease in NSE. The final iteration produced improvements in both indicators, in comparison with the

Table 2. Inflow Volume, Average Discharge, and Runoff Volume at Advance Times to the Middle of the Field, End of the Field, and Cutoff Time for the Printz 3-2-3 Example

t (min)	x (m)	V_{in} (m^3)	Q (L/s) (average)	V_{ro} (m^3)
27.0	175	4.86	3.00	0.00
63.5	350	13.46	3.53	0.00
110.0	350	24.74	3.75	1.13

J. Irrig. Drain Eng. 2012.138:727-735.
Downloaded from ascelibrary.org by Eduardo Bautista on 08/01/12. For personal use only.
No other uses without permission. Copyright (C) 2012. American Society of Civil Engineers. All rights reserved.

Table 3. Surface Shape Factors, Subsurface Shape Factors, Storage Volumes, Infiltrated Volumes, Estimated Infiltration Parameters, and Performance Indicators Computed at Each Volume-Balance Calculation Time and Iteration

t (min)	σ_y	σ_z	V_y (m^3)	V_z (m^3)	k (mm/h^a)	b (mm/h)	z (mm)	NSE
Iteration 1								
27	0.77	–	1.81	3.05				
63.5	0.77	–	4.07	9.38				
110	0.77	–	4.25	19.35	16.97	11.56	40	−1.62
Iteration 2								
27	0.720	0.643	1.67	3.19				
63.5	0.655	0.678	3.43	10.02				
110	0.726	0.796	4.00	19.61	9.68	17.86	42	0.84
Iteration 3								
27	0.696	0.615	1.61	3.25				
63.5	0.624	0.659	3.26	10.19				
110	0.675	0.799	3.71	19.90	13.63	15.23	42	0.38
Iteration 4								
27	0.705	0.630	1.63	3.23				
63.5	0.632	0.677	3.31	10.15				
110	0.689	0.789	3.79	19.81	9.90	18.15	43	0.90

results of the second and third iterations. The fact that the estimated parameters are very sensitive to the shape factors may help explain oscillations in the NSE value. In addition, the NSE indicator can be very sensitive when using short time series, as is the case in this example.

The accuracy of the solution ultimately depends on the accuracy of the inputs and the degree to which simulation-model assumptions are met in the field. With this important limitation in mind, it is still necessary to recognize that different infiltration solutions emerge, from the initial optimization problem to the last, and that, by the end of the process, the infiltrated volumes computed with Eq. (4) are closer to the simulated ones.

A final observation about this example is that the final solution, $k = 9.82$ mm/h$^{0.5}$ and $b = 18.15$ mm/h represents a soil for which the steady infiltration rate contributes a large fraction of the infiltration depth. An irrigation target of 50 mm, which is close to the applied and infiltrated depths from the field measurements, can be infiltrated in 2 h. The maximum advance distance that can be reached with $b = 18.15$ and $Q = 3.75$ L/s is 486 m, thus the field length (350 m) is over 70% of maximum length. These are the conditions under which the shape factors of the power infiltration integral can be inaccurate.

Conclusions

The power infiltration integral, derived by combining the Lewis-Milne integral equation with a power-law relationship for advance distance as a function of time, is more reliable when the ratio of average infiltration to upstream infiltration (σ_z) is a decreasing function of advance distance. Large steady-infiltration rates relative to the transient infiltration rate (λ), of the infiltration exponent a, and large field bottom slopes make the slope of the σ_z relationship positive at shorter relative advance distances, and thus make the power infiltration integral less accurate. The power-law integral can still yield reasonable infiltration estimates when the slope of σ_z is positive, but only if σ_z varies over a limited range. This is more likely when λ and S_0 are small, even for relative large values of a. In theory, the limitations of the power advance integral can be largely overcome by updating the value of r with increasing advance distance. This approach is limited by the erratic nature of field-measured advance data. A practical method for correcting these errors is by solving the volume-balance problem iteratively with the help of zero-inertia simulation. Subsurface shape factors (and surface shape factors) generated by the simulation can be used to update the volume-balance calculations.

Notation

The following symbols are used in this paper:

A_0 = upstream flow sectional area;
a = empirical infiltration exponent;
BW = bottom width for a trapezoidal furrow;
b = empirical infiltration steady-infiltration rate constant;
E_{VB} = volume-balance error;
FS = furrow spacing;
k = empirical infiltration constant;
L_f = field length;
n = Manning roughness coefficient;
p = power advance constant;
Q_0 = inflow rate;
R = hydraulic radius;
RZ_1, RZ_2 = shape factors of the power-law infiltration integral;
r = power advance exponent;
S_f = friction gradient;
S_0 = field bottom slope;
SS = side slope for a trapezoidal furrow;
t = time;
t_{req} = time required to infiltrate the required infiltration depth z_{req};
t_x = advance time to distance x;
V_{in} = inflow volume;
V_{RO} = runoff volume;
V_y = surface storage volume;
V_Z = infiltration volume;
x_A = advance distance;
y = flow depth;
y_n = normal flow depth;
y_0 = upstream flow depth;
Z = infiltration volume per unit length;
z = infiltration volume per unit area;
z_{req} = required infiltration depth;
λ = relative contribution of the steady-state infiltration term to z_{req} in t_{req};
σ_Y = surface shape factor; and
σ_z = ratio of average and upstream infiltration volume per unit length computed by zero-inertia simulation.

References

Bautista, E., Clemmens, A. J., and Strelkoff, T. S. (2009a). "Optimal and postirrigation volume balance infiltration parameter estimates for basin irrigation." *J. Irrig. Drain. Eng.*, 135(5), 579–587.

Bautista, E., Clemmens, A. J., and Strelkoff, T. S. (2009b). "Structured application of the two-point method for the estimation of infiltration parameters in surface irrigation." *J. Irrig. Drain. Eng.*, 135(5), 566–578.

Bautista, E., Clemmens, A. J., Strelkoff, T. S., and Schlegel, J. (2009c). "Modern analysis of surface irrigation systems with WinSRFR." *Agric. Water Manage.*, 96(7), 1146–1154.

J. Irrig. Drain Eng. 2012.138:727-735.
Downloaded from ascelibrary.org by Eduardo Bautista on 08/01/12. For personal use only.
No other uses without permission. Copyright (c) 2012. American Society of Civil Engineers. All rights reserved.

Bautista, E., Strelkoff, T. S., and Clemmens, A. J. (2012). "Improved surface volume estimates for surface irrigation volume-balance calculations." *J. Irrig. Drain. Eng.*, 138(8), 715–726.

Bautista, E., and Wallender, W. W. (1993). "Numerical calculation of infiltration in furrow irrigation simulation models." *J. Irrig. Drain. Eng.*, 119(2), 286–294.

Christiansen, J. E., Bishop, A. A., Kiefer, F. W., Jr., and Fok, Y.-S. (1966). "Evaluation of intake rate constants as related to advance of water in surface irrigation." *Trans. Am. Soc. Agric. Eng.*, 9(5), 671–674.

Elliott, R. L. (1980). "Furow irrigation field evaluation data. Summers of 1977–1979." *Internal Rep., Dept. of Agricultural and Chemical Engineering*, Colorado State Univ., Fort Collins, CO.

Elliott, R. L., and Walker, W. R. (1982). "Field evaluation of furrow infiltration and advance functions." *Trans. Am. Soc. Agric. Eng.*, 25(2), 396–400.

Furman, A., Warrick, A. W., Zerihun, D., and Sanchez, C. A. (2006). "Modified Kostiakov infiltration function: Accounting for initial and boundary conditions." *J. Irrig. Drain. Eng.*, 132(6), 587–596.

Lewis, M. R., and Milne, W. E. (1938). "Analysis of border irrigation." *Agric. Eng.*, 19(6), 267–272.

McClymont, D. J., and Smith, R. J. (1996). "Infiltration parameters from optimisation on furrow irrigation advance data." *Irrig. Sci.*, 17(1), 15–22.

Nash, J. E., and Sutcliffe, J. V. (1970). "River flow forecasting through conceptual models part I—A discussion of principles." *J. Hydrol.*, 10(3), 282–290.

Philip, J. R., and Farrell, D. A. (1964). "General solution of the infiltration-advance problem in irrigation hydraulics." *J. Geophys. Res.*, 69(4), 621–631.

Scaloppi, E. J., Merkley, G. P., and Willardson, L. S. (1995). "Intake parameters from advance and wetting phases of surface irrigation." *J. Irrig. Drain. Eng.*, 121(1), 57–70.

Smerdon, E. T., Blair, A. W., and Reddell, D. L. (1988). "Infiltration from irrigation advance data. I: Theory." *J. Irrig. Drain. Eng.*, 114(1), 4–17.

Strelkoff, T. S., Clemmens, A. J., and Bautista, E. (2009). "Estimation of soil and crop hydraulic properties." *J. Irrig. Drain. Eng.*, 135(5), 537–555.

Trout, T. J. (1992). "Flow velocity and wetted perimeter effects on furrow infiltration." *Trans. Am. Soc. Agric. Eng.*, 35(3), 855–863.

Valiantzas, J. D., Pollalis, E. D., Soulis, K. X., and Londra, P. A. (2009). "Modified form of the extended Kostiakov equation including various initial and boundary conditions." *J. Irrig. Drain. Eng.*, 135(4), 450–458.

Walker, W. R., and Kasilingam, B. (2004). "Another look at wetted perimeter along irrigated furrows—Modeling implications." *Proc., 2004 World Water and Environmental Resources Congress for Critical Transitions in Water and Environmental Resources Management*, ASCE, Reston, VA, 1664–1670.

Walker, W. R., Prestwich, C., and Spofford, T. (2006). "Development of the revised USDA-NRCS intake families for surface irrigation." *Agric. Water Manage.*, 85(1–2), 157–164.

J. Irrig. Drain Eng. 2012.138:727-735.
Downloaded from ascelibrary.org by Eduardo Bautista on 08/01/12. For personal use only.
No other uses without permission. Copyright (c) 2012. American Society of Civil Engineers. All rights reserved.